Electronic Supplementary Material (ESI) for Chemical Communications.

Supplementary Information

Quick mass-production of MAX (Ti_2AlC) book with pages separated by stacking faults benefiting removal of “A” layer

Chaozhong Wu,[a] Ruifeng Qi,[a] Xiong Zhang,[b] Qiang Liu,[a] Qingsong Huang*[a]

[a] School of Chemical Engineering, Sichuan University, Chengdu 610065, China
[b] Institute of Chemistry and Processes for Energy, Environment and Health (ICPEES)，UMR 7515 CNRS，University of Strasbourg (UdS)，25 rue Becquerel, 67087 Strasbourg Cedex 02, France
*Corresponding e-mail: qshuang@scu.edu.cn

1. The flow of the vortex currents cause stacking faults between layers and the magnetism and vortext current coupling growth (MVC) technique

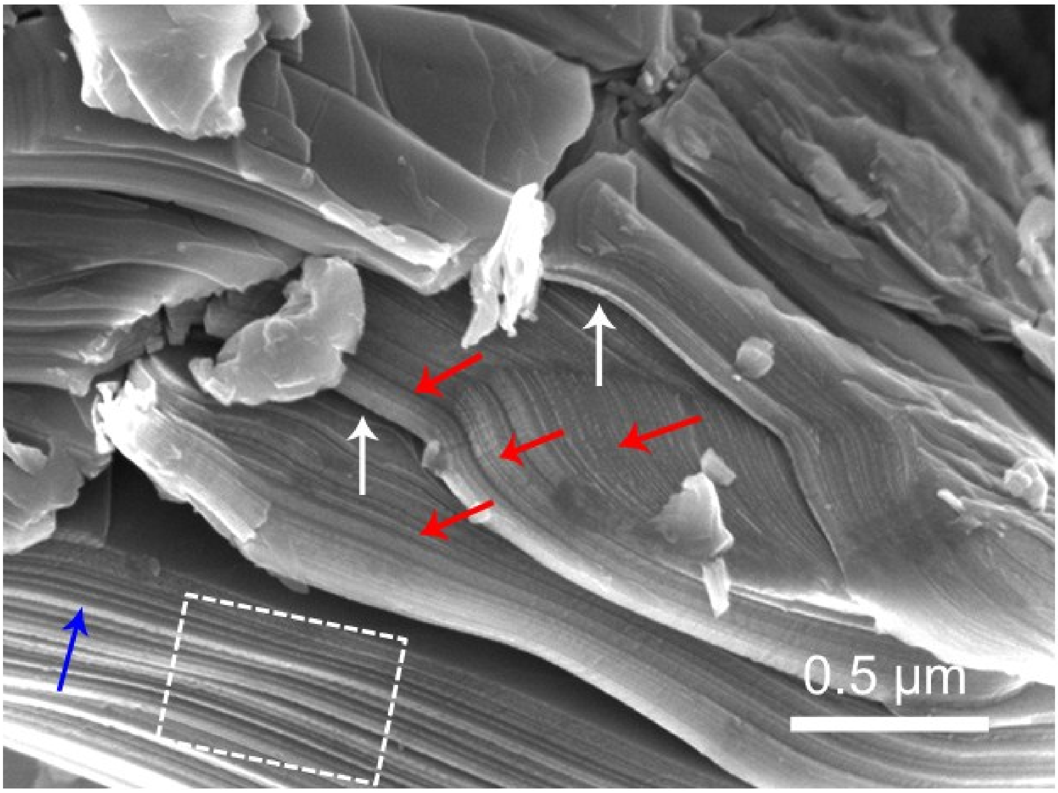

Fig. S1 (Color online) The morphology of the Ti_2AlC. The dashed frame and arrows (white and red) display the stacking faults and vortex current trace. The pointed CR-Layer by blue arrow arises from cooling of R-Layer.

If the sintering proceeds fully, some of the layers can be ejected from the “book”, and the layer surface is etched into streamlines by the flowing current flux (Fig. S1 red arrows), while the stacking faults have been etched into the cleavage gap (Fig. S1 white arrows and dashed frame).

1.1 The description for the magnetism and vortext current coupling growth (MVC) technique

The MVC is abbreviated from magnetism and vortex current coupling growth.
When magnetic flux penetrates the sample, the induction vortex electric field will circle the flux immediately, triggering many localized eddy current, and the sample was heated by the eddy currents.
The eddy currents are illustrated as Fig. 1(c), showcasing the localized eddy currents.
The eddy currents can heat the entire sample simultaneously. With the temperature arising, the heated samples become conducting finally, the eddy current become connected each other and flowing along the edge brim into vortex current, heating more efficiently.

The graphite paper has been adopted to heat the sample R-Layer (Fig. S1) one by one gradually.
The graphite paper as heating source turns to red color. Alongside, the eddy current arising from the alternating magnetic field can heat the sample too. The R-layer next to the heating source can be activated into vortex current, arising from the connection of eddy current and propagating to center next. After that, the layer next to the R-Layer turns to red as well, and so forth. Finally, the pressed block forms into Ti_2AlC stacked layer by layer (Fig. S1).

2. Fingerprint of our layered MAX after manual grinding

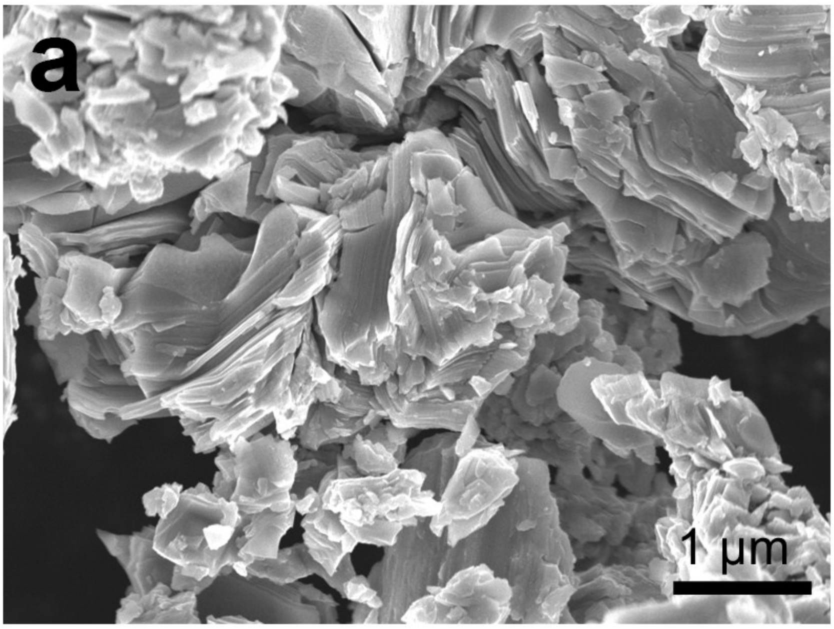

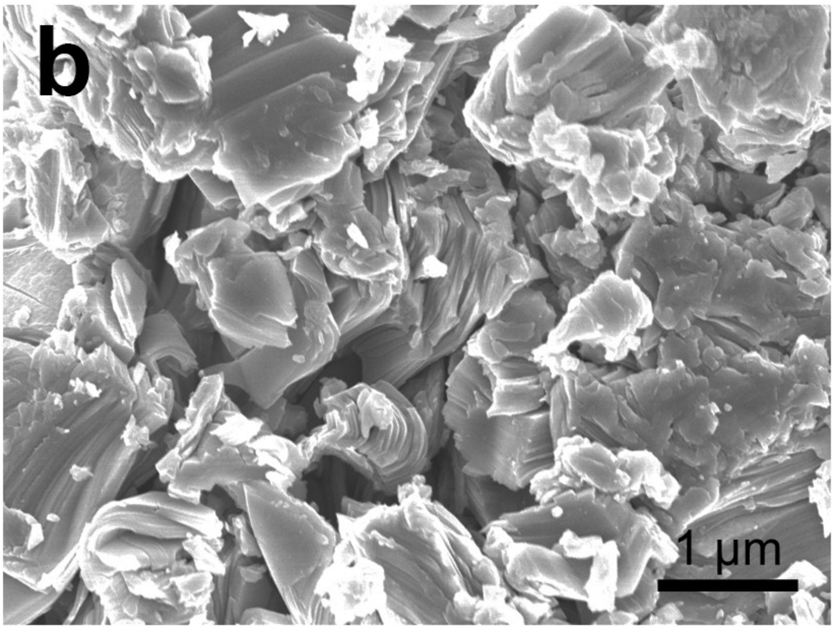

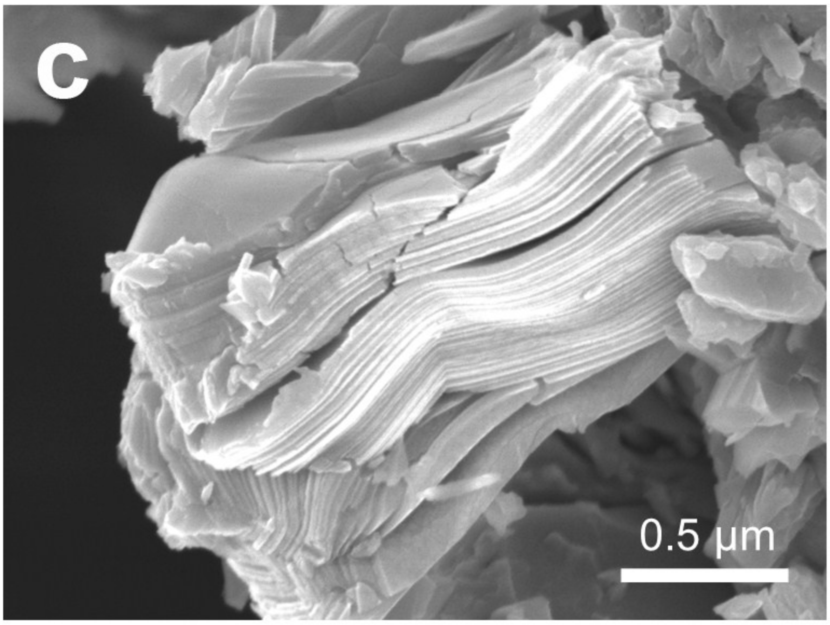
c
0.5 µm

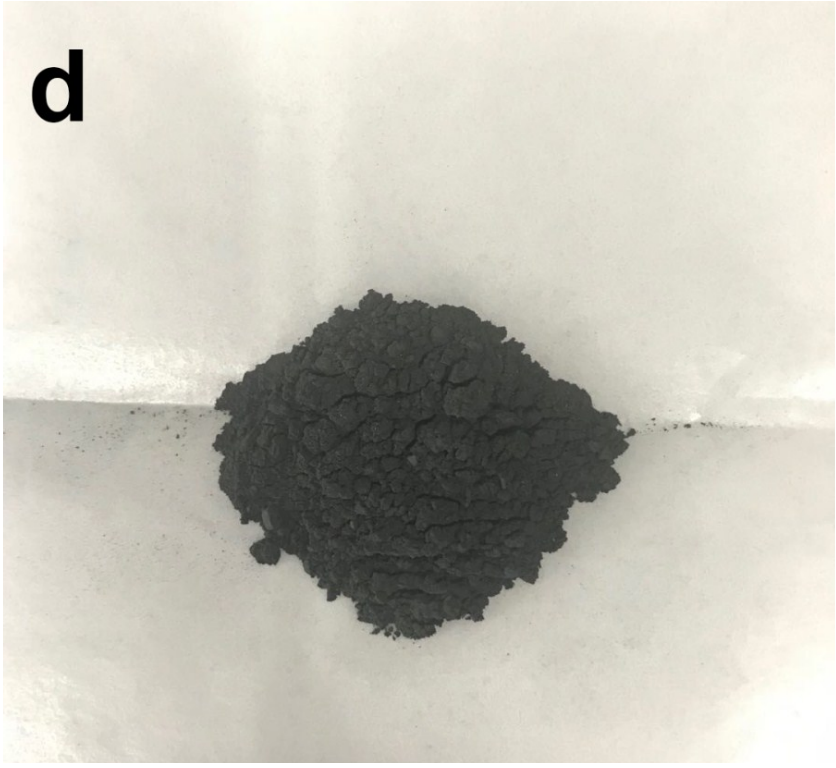
d

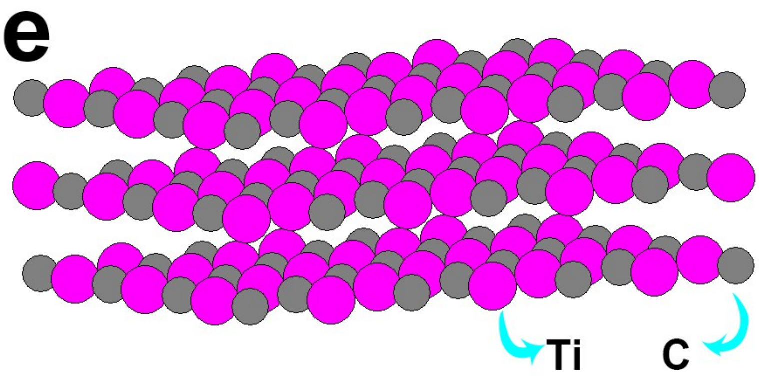

Figure S2. The morphology of our layered MAX phase after manual grinding, (a) its size distributions, (b) collecting from the MAX phase randomly and (c) the typical characteristics alongside. (d) Picture of gram-scale real products by our MVC technique and (e) the schematic structure of TiC (PDF#65-8805).

The MAX phase is estimated to be around a micrometer (Fig. S2), enabling the layered structure to be viewed from most particles.

3. The XRD of the sintering Ti_2AlC (Ti, Al and C powders mixed in a non-stoichiometric ratio of 3:2:1)

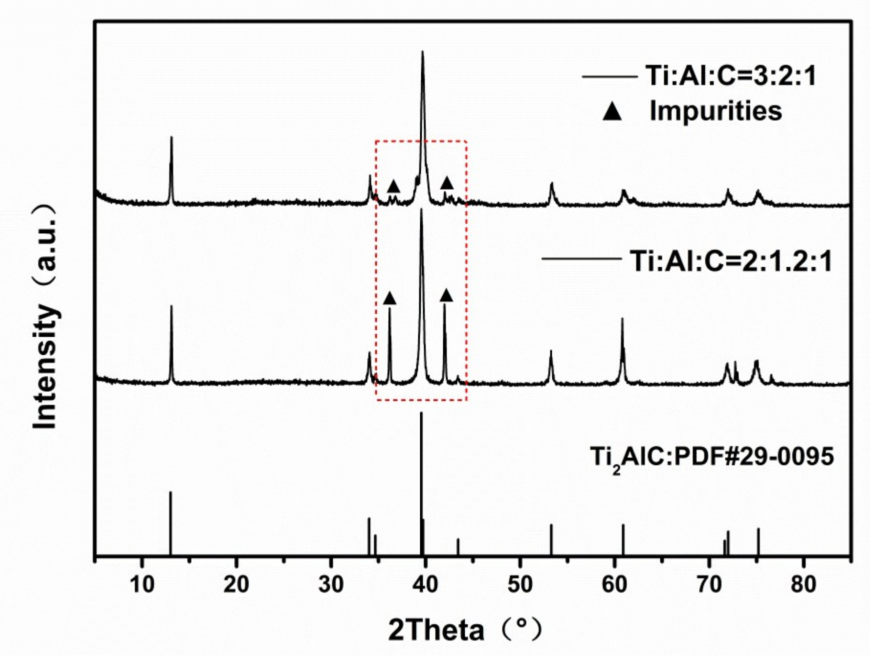

Figure S3. The Ti, Al and C powders are mixed in a non-stoichiometric ratio of 3:2:1 for sintering Ti_2AlC, where intensities of TiC-phase peaks decrease markedly and triangles represent the impurities.

4. Synthisizing V_2AlC MAX-phase by the magnetism and vortex current coupling growth (MVC) technique

Fig. S4(a) is the XRD pattern of V_2AlC, corresponding to PDF#29-0101, where the strongest peak is at 41.2° and the (002) characteristic peak is at 13.4°, and the secondary phase is VO, at approximately 37.8° and 43.9°. The XRD spectra of powder diffraction demonstrate the obtained MAX phase of V_2AlC approaches pure phase with very small impurity peak (Fig. S4(a) red spectrum marked with black triangles). The lamellae structure can be realized as well. The MAX phase stacked layer by layer can be viewed in Fig. S4(b).

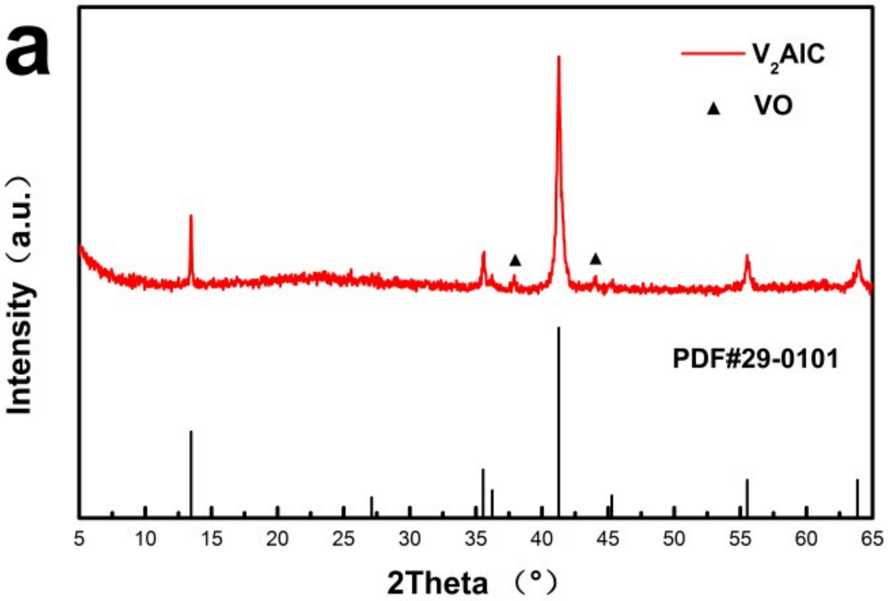

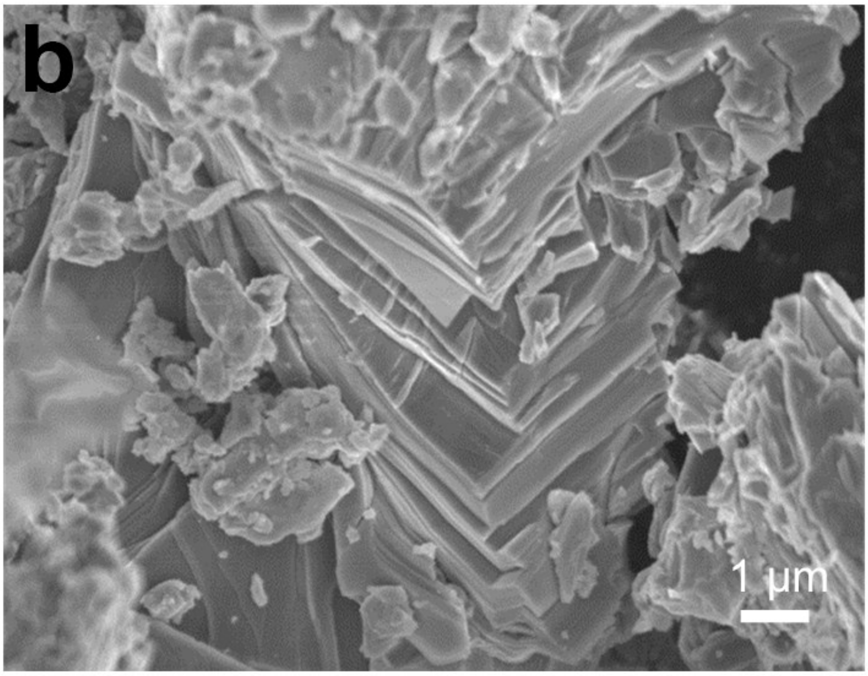

Fig. S4 (Color online) The characterizations of the MVC technique for ultra-rapidly preparing the V_2AlC phase. (a) The XRD pattern and (b) The SEM image of V_2AlC.

5. The XRD of the sintering Ti_2AlC (Ti, Al and C powders mixed in a non-stoichiometric ratio of 2:1.2:1)

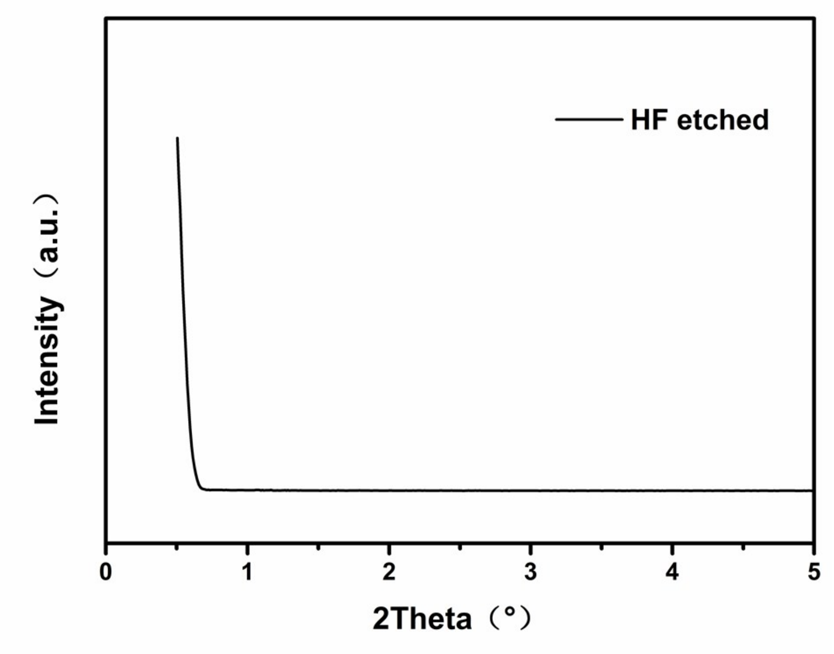

Fig. S5 The Small Angle X-ray Scattering pattern of the Ti_2AlC after 10% HF treatment for 1 h.

6. Schematic of heating process and the MAX phase etched by HF for different time

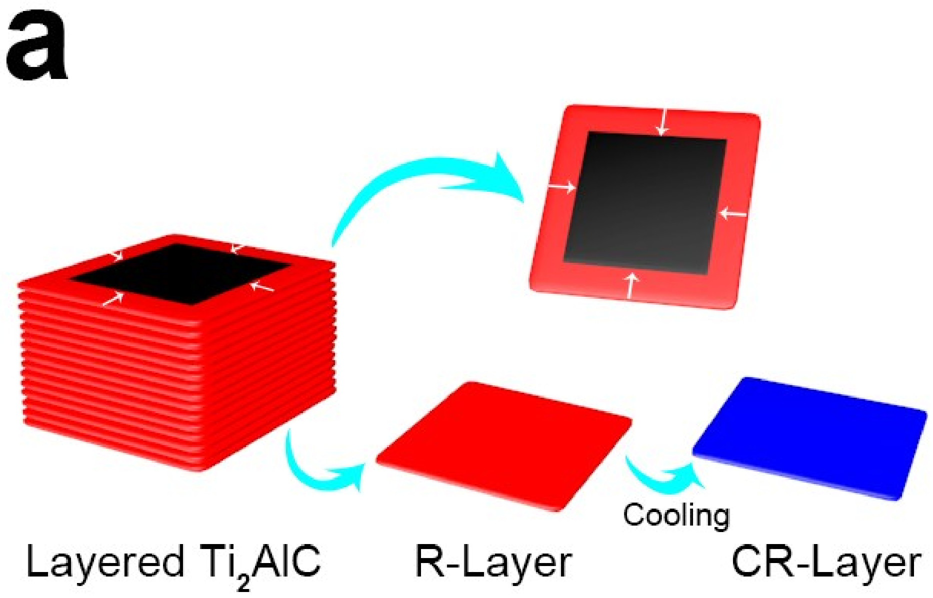

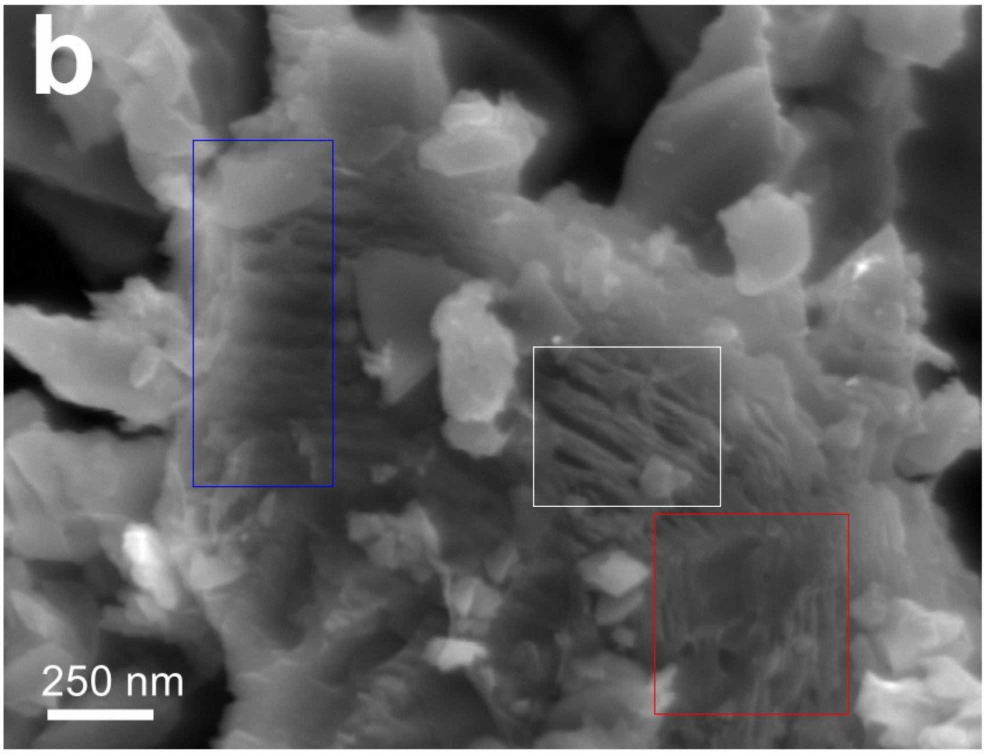

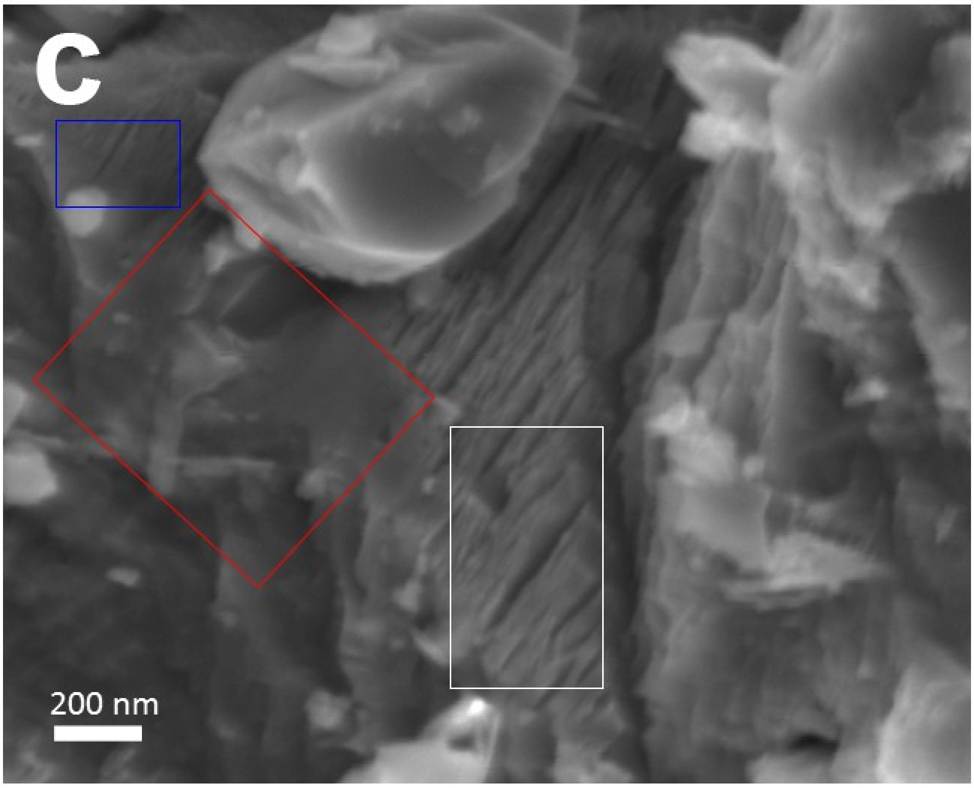
c
200 nm

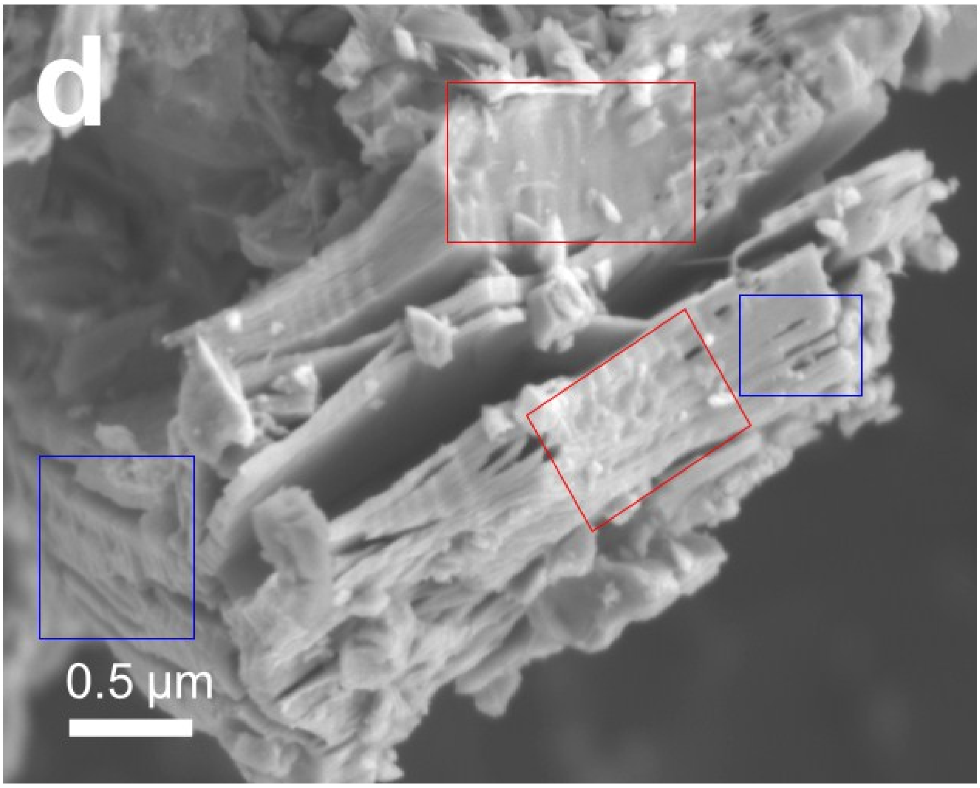
d
0.5 µm

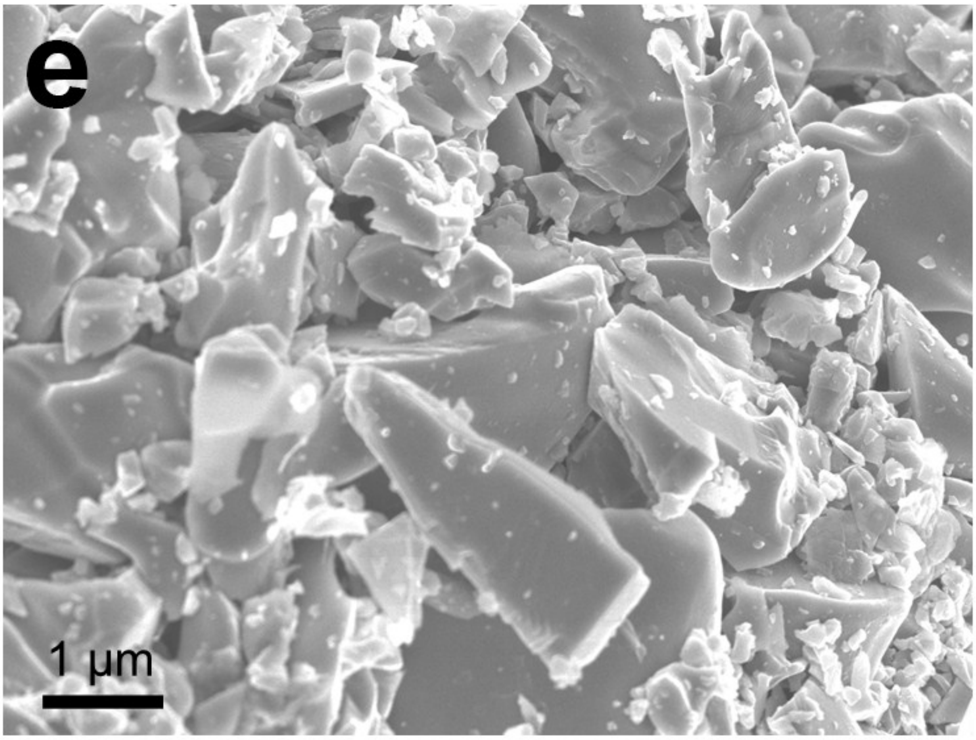

Fig. S6 (Color online) (a) Schematic of R-Layer and CR-Layer. When the R-Layer is heating, the fringe alongside the wafer turns red first, propagating to center successively. The MAX phase of Ti_2AlC after 10% HF treatment for 2 h (b,c), 3 h (d) and 10 h (e).

For the size of those red layers, refer to Fig. S1, Fig. 2(c) and 3(a). Some of the defects can be inherited by the MXene, and enhance the adsorption ability on the surface (Fig. 3(b)).

6.1. The description for the assumptive growth mechanism of the Ti_2AlC

In Fig. 2(e) left, when the magnetic field lines of flux penetrate the sample, the induced eddy currents can be generated locally, by which the Ti, Al, C powders are heated and blended.

In addition, the intensity of magnetization distributes depending on the Z axis (001) orientation, because the densities of magnetic lines of flux change with height. Ideally, the eddy currents display stratified distribution, and the layer immediate next to R-Layer (heating layer) will be heated to red, if the local eddy currents developed into a vortex recycling current alongside the wafer.

According to thus mechanism, from the bottom to top, the vortex current layers can be lightened up (becoming red) in turn, and becomes layered Ti_2AlC phase (Fig. 2(e) right, Fig. S6(a)).

6.2. The description for the etching process of the Ti_2AlC

On the interface of the CR-layers, the etching proceeds quickly because of the defects and the stacking faults (Fig. S1,), but when the etching time is prolonged, the left M layers and X layers could be damaged or etched out. Meanwhile, the A layers become more difficult to etch because the A layers have been masked by the damaged M layers and X layers (Fig. S6). So the typical Ti_2CT_x MXene lamellae disappear gradually if the etching time is extended from 2 h to 10 h (Fig. S6(b–e)), losing the lamellar structure partly (Fig. S6(b-d)) and then completely (Fig. S6(e)), because of the excessive corrosion or etching defects from the specific heating of the R-layers.

In Fig. S6(b-d), white frame, blue frame and red frame show the process of structural corrosion when the etching time is from 2 h to 3h, and Ti_2CT_x MXene lamellae will disappear completely finally if the etching time is extended to 10h in Fig. S6(d).

7. The MAX phase etched by different ways

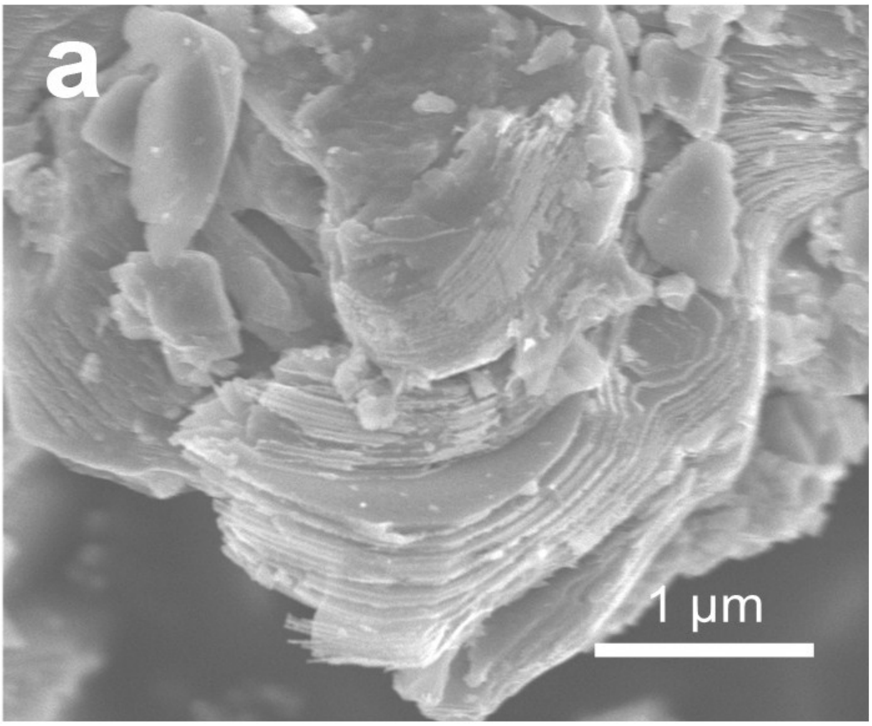

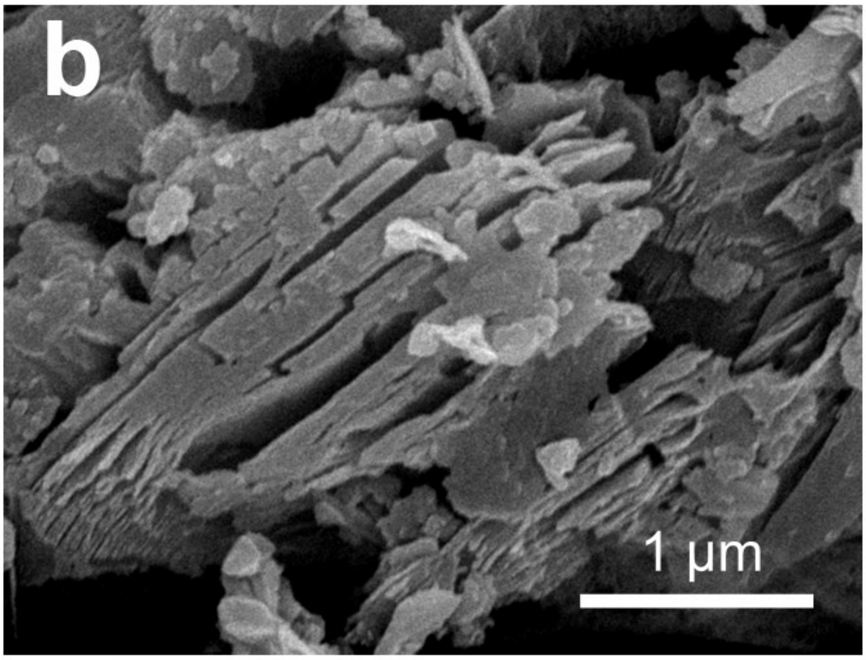

Fig. S7 Exfoliation of Ti_2AlC (MAX phase) undergoing (a) 10% HF treatment for 30 min and (b) 5% HF treatment for 2 h.

If the etching time is shortened to 30 min, the etching cannot proceed fully, but the layered MXene phase has been achieved (Fig. S7(a)). Even if the concentration of hydrofluoric acid is reduced to 5% in weight, the layered MXene phase can still be obtained (Fig. S7(b)).

8. TEM images of Ti_2CT_x MXene (after 10% HF treatment for 1 h)

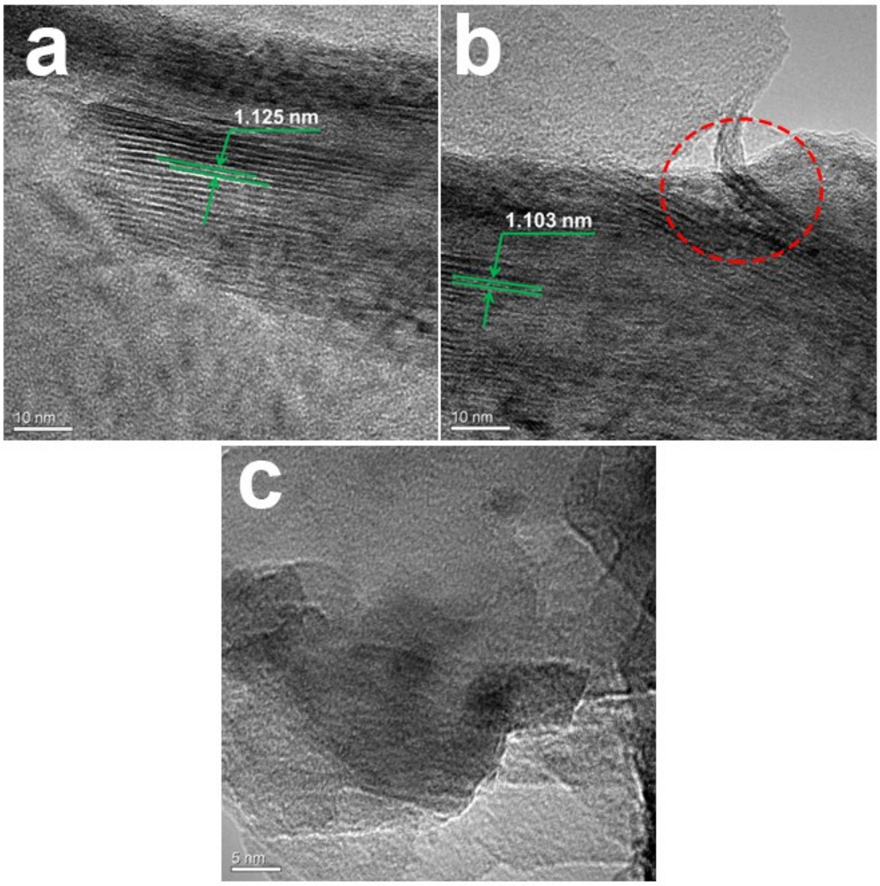

Fig. S8 (a), (b) and (c) The another TEM images to clarify the Ti_2CT_x MXene layered structure.

An additional TEM characterization has been performed clarify the layered structure of MXene composing of CR-layers. The inter-distance of *ca.* 1.1 nm between the adjacent layers suggests the A-layer has been etched out by HF (10%) (Fig. 8(a,b)). The layered structure can also be viewed from the left top in Fig. 8(b) and Fig. 8(c). The layers are vulnerable to be seperated because of the weak van der Waals interactions between adjacent layers, refering to the Fig.8(b) red circle, and Fig. 8(c).

9. XPS and Raman analyses for Ti_2AlC before and after HF treatment

XPS analysis: XPS spectrum has been adopted to determine the chemistry of the Ti_2AlC phase after HF treatment. The survey spectrum of Ti_2CT_x illustrates the Ti, C, O, and F elements are all available (Fig. S9(a)). The content of Al element cannot almost be identified and ignorable (Fig. S9(a)), suggesting Al is selectively etched away. High-resolution Ti 2p spectrum peak shows the binding energy 454.4 eV, 455.5 eV. 456.5 eV, 457.6 eV, 458.8 eV of the Ti $2p_{3/2}$ components in Fig. S9(b). The binding energy 458.8 eV corresponds to Ti^{4+} ion,[1, 2] the intensity ratio of which is larger than Ti-C bond compared to the previous literature.[3] The binding energy in 456.5 eV and 457.6 eV belong to Ti_xO_y, in particular, the binding energy 456.5 eV is related to Ti^{3+} ion.[1-3] However, no Ti-O_x structures can be identified in the XRD, implying the oxygen has not formed into crystal structure, but adsorbed on the surface of our MVC-MXene only. At the same time, these peaks to Ti-O bonds imply the adsorption ability on our MXene surface is forceful.[4, 5] The Ti $2p_{3/2}$ component centered at 454.4 eV is assigned to Ti-C bond,[2, 6] and 455.5 eV to Ti-X bond (a combination of TiC_x and TiC_xO_y),[2, 3] which determines the generation of Ti_2CT_x further. Fig. S9(c) shows a high-resolution C 1s components locat at 281.4 eV, 282.2 eV, 284.8 eV, 286.4 eV, 288.8 eV, where those binding energies correspond to C-Ti,[3, 7, 8] C-Ti-O, C-C, C-O,[3, 8, 9] O-C=O and C-F bonds,[3, 9, 10] respectively.

Raman analyses: Raman scattering has been performed to identify the MAX and MXene (Fig. S9(d)). The peaks at ω_1, ω_2 & ω_3 and ω_4 are due to the vibration of Al and Ti atoms,[11-14] and ω_6 and ω_7 correspond to the D peak and G peak of soild carbon.[12, 13] Because no XRD peaks are found for the characteristic peaks of graphite, suggesting the D peak and G peak of C in Raman spectra is due to the small amount of amorphous C from as-received raw material powders. The peak at about 145 cm^{-1} after HF etching is due to a small amount of Ti_xO_y referring to Fig. S9(b).[3, 8, 15] The other three Raman peaks belong to the nonstoichiometric titanium carbide.[3, 16, 17] Whereas, when the MAX changes to MXene, the layered Ti_2C makes the in-plane phonon vibration enhanced and the intensity of Raman peaks increasing ((Fig. S9(d)) red spectrum).

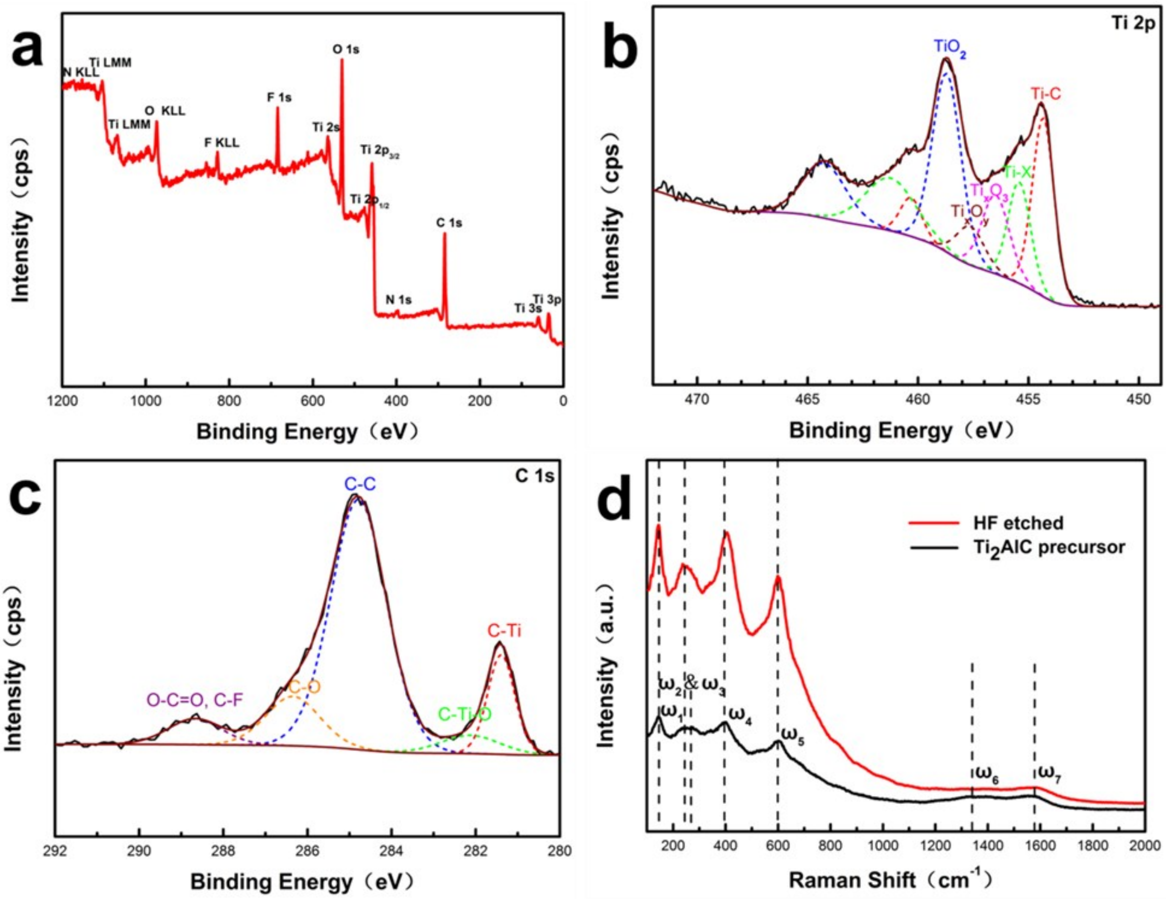

Fig. S9 (Color online) XPS survey and Raman scattering for chemistry of the MAX phase and MXene. (a) The survey spectrum, (b) high-resolution Ti 2p spectrum and (c) high-resolution C 1s spectrum of the Ti_2AlC after 10% HF treatment for 1 h. (d) Raman spectra of the Ti_2AlC before and after 10% HF treatment for 1 h. (ω_1: the vibration of Al atom; ω_2 & ω_3 and ω_4: the vibration of Ti atom; ω_6 and ω_7: the D&G peak of C)

10. Comparison for Ti_2AlC after HF treatment

Tab. S1 Li-ion storage performance of different Ti_2CT_x electrodes

Type of material	Capacity (mAh g^{-1})	Cycling stability (mAh g^{-1})	Reference
Ti_2CT_x	83.2	~ 140 (After 525 cycles at 100 mA g^{-1})	This work
–	–	93.6 (After 200 cycles at 100 mA g^{-1})	Ref. 18
exfoliated Ti_2C	–	110 (After 80 cycles at 1C)	Ref. 19
Ti_2C	–	~ 150 (After 20 cycles at C/5)	Ref. 20

11. Fabrication of MAX phases by MVC technique and Ti_2AlC etched by HF

Synthesis of Ti_2AlC: Ti (Fengyue, Tianjin, China, 99.99 wt %, -400 mesh), Al (Chengdu, China, 99 wt %, -325 mesh) and C (Alanddin Industrial Corporation, China, 99.95 wt %, -325 mesh) are mixed in a non-stoichiometric ratio of 2:1.2:1 or 3:2:1 by ball mill for 30 minutes and excess Al is used to balance the volatilization of Al at high temperature. The certain amount powders after ball milling are pressed into a cylindrical shape by the oil press. Next the pressed block was placed in an alumina crucible and heated with graphite paper or graphite sheet as a heating source in a magnetic suspension melting furnace which was filled with argon. Then the pressed block is preheated for 30 s at a power of 26.0 KW by this furnace. After that, the block is heated for 20 s by means of adjusting the power of this furnace to 30.0 KW. After removing the surface impurities, the obtained bulk can be grounded with a diamond drill to obtain the powders, screening *via* a -500 mesh sieve for as-received powders.

Synthesis of V_2AlC: V (Fengxian, Shanghai, China, 99.5 wt %, -325 mesh), Al (Chengdu, China, 99 wt %, -325 mesh) and C (Alanddin Industrial Corporation, China, 99.95 wt %, -325 mesh) are ball milled at a non-stoichiometric ratio of 2:1.2:1 and then pressed into a cylinder. Next, the cylinder is preheated for 30 s at a power of 26.0 KW by this furnace and heated for 5 s by means of adjusting the power of this furnace to 30.0 KW. The sintered bulk was ground into a powder and sieved through a -500 mesh sieve for the next experiment. Synthesis of V_2AlC follows the above Ti_2AlC.

Synthesis of Ti_2CT_x: The as-prepared Ti_2AlC powders over -500 mesh sieve was magnetically stirred in 10% HF solution at room temperature for 1 h. After that, the precipitate arising from the solution by centrifugation was washed with deionized water at 3500 rpm for 5 minutes by the high speed centrifuge till the pH value of the suspension was about 6. Finally the precipitate was dried in a freeze dryer for 12 hours to obtain the Ti_2CT_x powders.

12. Materials characterization and electrochemical measurement

Characterization of the samples: Materials characterization was measured by SEM (JEOL JSM-7800F equipped with EDS), TEM (JEM-2100), XRD (Bruker D8 ADVANCE A25X using Cu Kα radiation.), Small Angle X-ray Scattering (SAXS, X'Pert Pro MPD, Cu target, post graphite monochromator), XPS (Thermo ESCALAB 250Xi equipped with monochromatic Al Kα source) and Raman spectroscopy (HORIBA) at 455 nm laser excitation.

Electrochemical Measurement: 80 wt % of Ti_2CT_x, 10 wt % of acetylene black and 10 wt % of Poly(vinylidene fluoride) were uniformly mixed with NMP (N-methyl-2-pyrrolidone) and coated on the copper foil, and then dried in a vacuum oven at 80 °C for 12 h. The active material on a copper foil as the positive electrode was measured about 0.8-1 mg cm^{-2}, the diameter of which is 12 mm, and the negative electrode is lithium foil. Then they are assembled into a CR2032-type button battery in a glove box filling argon with the concentrations of water and oxygen less than 1 ppm, separated by a separator Celgard 2325. The button battery, which is filled with 1M lithium hexafluorophosphate as the solute and EC:DEC:DMC in a volume ratio of 1:1:1 as the solvent, is allowed to put overnight and the electrochemical performance is tested with the Neware test system in the voltage range of 0.005-3.0 V. The CV performance curve is measured by CHI 660E type electrochemical workstation in the voltage range of 0.005-3.0 V (vs. Li^+/Li).

References

1. M. C. Biesinger, L. W. M. Lau, A. R. Gerson and R. S. C. Smart, *Appl. Surf. Sci.*, 2010, **257**, 887-898.
2. M. M. Ottakam Thotiyl, S. A. Freunberger, Z. Peng, Y. Chen, Z. Liu and P. G. Bruce, *Nat. Mater.*, 2013, **12**, 1050-1056.
3. B. Ahmed, D. H. Anjum, M. N. Hedhili, Y. Gogotsi and H. N. Alshareef, *Nanoscale*, 2016, **8**, 7580-7587.
4. Q. Peng, J. Guo, Q. Zhang, J. Xiang, B. Liu, A. Zhou, R. Liu and Y. Tian, *J. Am. Chem. Soc.*, 2014, **136**, 4113-4116.
5. T. Y. Ma, X. J. Zhang, G. S. Shao, J. L. Cao and Z. Y. Yuan, *J. Phys. Chem. C*, 2008, **112**, 3090-3096.
6. B. H. Q. Dang, M. Rahman, D. Macelroy and D. P. Dowling, *Surf. Coat. Technol.*, 2011, **205**, S235-S240.
7. S. Yoon and A. Manthiram, *Electrochim. Acta*, 2011, **56**, 3029-3035.
8. F. Dong, H. Wang and Z. Wu, *J. Phys. Chem. C*, 2009, **113**, 16717-16723.
9. L. Zhang, G. Chen, M. N. Hedhili, H. Zhang and P. Wang, *Nanoscale*, 2012, **4**, 7038-7045.
10. H. Touhara and F. Okino, *Carbon*, 2000, **38**, 241-267.
11. V. Presser, M. Naguib, L. Chaput, A. Togo, G. Hug and M. W. Barsoum, *J. Raman Spectrosc.*, 2012, **43**, 168-172.
12. S. A. Melchior, K. Raju, I. S. Ike, R. M. Erasmus, G. Kabongo, I. Sigalas, S. E. Iyuke and K. I. Ozoemena, *J. Electrochem. Soc.*, 2018, **165**, A501-A511.
13. F. Liu, A. Zhou, J. Chen, H. Zhang, J. Cao, L. Wang and Q. Hu, *Adsorption*, 2016, **22**, 915-922.
14. J. E. Spanier, S. Gupta, M. Amer and M. W. Barsoum, *Phys. Rev. B*, 2005, **71**, 012103.
15. V. Swamy, A. Kuznetsov, L. S. Dubrovinsky, R. A. Caruso, D. G. Shchukin and B. C. Muddle, *Phys. Rev. B*, 2005, **71**, 184302.
16. B. H. Lohse, A. Calka and D. Wexler, *J. Alloys Compd.*, 2007, **434**, 405-409.
17. K. J. Cai, Y. Zheng, P. Shen and S. Y. Chen, *Crystengcomm*, 2014, **16**, 5466-5474.
18. L. Li, F. Wang, J. Zhu and W. Wu, *Dalton Trans.*, 2017, **46**, 14880-14887.

19. M. Naguib, J. Come, B. Dyatkin, V. Presser, P.-L. Taberna, P. Simon, M. W. Barsoum and Y. Gogotsi, *Electrochem. Commun.*, 2012, **16**, 61-64.
20. J. Come, M. Naguib, P. Rozier, M. W. Barsoum, Y. Gogotsi, P. L. Taberna, M. Morcrette and P. Simon, *J. Electrochem. Soc.*, 2012, **159**, A1368-A1373.